

# Partially Observed Dynamic Tensor Response Regression

Jie Zhou\*, Will Wei Sun<sup>†</sup>, Jingfei Zhang<sup>‡</sup> and Lexin Li<sup>§</sup>

## Abstract

In modern data science, dynamic tensor data is prevailing in numerous applications. An important task is to characterize the relationship between such dynamic tensor and external covariates. However, the tensor data is often only partially observed, rendering many existing methods inapplicable. In this article, we develop a regression model with partially observed dynamic tensor as the response and external covariates as the predictor. We introduce the low-rank, sparsity and fusion structures on the regression coefficient tensor, and consider a loss function projected over the observed entries. We develop an efficient non-convex alternating updating algorithm, and derive the finite-sample error bound of the actual estimator from each step of our optimization algorithm. Unobserved entries in tensor response have imposed serious challenges. As a result, our proposal differs considerably in terms of estimation algorithm, regularity conditions, as well as theoretical properties, compared to the existing tensor completion or tensor response regression solutions. We illustrate the efficacy of our proposed method using simulations, and two real applications, a neuroimaging dementia study and a digital advertising study.

**Key Words:** Alzheimer’s disease; Digital advertising; Neuroimaging analysis; Non-convex optimization; Tensor completion; Tensor regression.

---

\*PhD student, Department of Management Science, University of Miami Herbert Business School, Miami, FL 33146. Email: jzhou@bus.miami.edu.

<sup>†</sup>Assistant Professor, Krannert School of Management, Purdue University, IN 47907. Email: sun244@purdue.edu.

<sup>‡</sup>Assistant Professor, Department of Management Science, University of Miami Herbert Business School, Miami, FL 33146. Email: ezhang@bus.miami.edu.

<sup>§</sup>Professor, Division of Biostatistics, University of California, Berkeley, Berkeley, CA 94720. Email: lexinli@berkeley.edu.

# 1 Introduction

In modern data science, dynamic tensor data is becoming ubiquitous in a wide variety of scientific and business applications. The data takes the form of a multidimensional array, and one mode of the array is time, giving the name dynamic tensor. It is often of keen interest to characterize the relationship between such time-varying tensor data and external covariates. One example is a neuroimaging study of Alzheimer’s disease (AD) (Thung et al., 2016). Anatomical magnetic resonance imaging (MRI) data are collected for 365 individuals with and without AD every six month over a two-year period. Each image, after preprocessing, is of dimension  $32 \times 32 \times 32$ , and the combined data is in the form of a subject by MRI image by time tensor. An important scientific question is to understand how a patient’s structural brain atrophy is associated with clinical and demographic characteristics such as the patient’s diagnosis status, age and sex. Another example is a digital advertising study (Bruce et al., 2017). The click-through rate (CTR) of 20 active users reacting to digital advertisements from 2 publishers are recorded for 80 advertisement campaigns on a daily basis over a four-week period. The data is formed as a tensor of campaign by user by publisher by time. An important business question is to understand how features of an advertisement campaign affect its effectiveness measured by CTR on the target audience. Both questions can be formulated as a supervised tensor learning problem. However, a crucial but often overlooked issue is that the data is likely only partially observed in real applications. For instance, in the neuroimaging study, not all individuals have completed all five biannual MRI scans in two years. In the digital advertising study, not all users are exposed to all campaigns, nor react to all publishers. Actually, in our digital advertising data, more than 95% of the entire tensor entries are unobserved. In this article, we tackle the problem of supervised tensor learning with partially observed tensor data.

There are several lines of research that are closely related to but also clearly distinctive of the problem we address. The first line studies tensor completion (Jain and Oh, 2014; Yuan and Zhang, 2016, 2017; Xia and Yuan, 2017; Zhang, 2019). Tensor completion aims to fill in the unobserved entries of a partially observed tensor, usually by resorting to some tensor low-rank and sparsity structures. It is unsupervised learning, as it involves no external covariates. While we also tackle tensor with unobserved entries and we are to employ similar

low-dimensional structures as tensor completion, our goal is not to complete the tensor. Instead, we target a supervised learning problem, and aim to estimate the relationship between the partially observed tensor and the external covariates. Consequently, our model formulation, estimation approach, and theoretical analysis are considerably different from tensor completion. The second line studies regressions with matrix or tensor-valued response. Specifically, [Zhu et al. \(2009\)](#) proposed an intrinsic regression model for a positive-definite matrix-valued response and a vector of covariates, by mapping the Euclidean space of the covariates to the Riemannian manifold of the positive-definite matrix. [Rabusseau and Kadri \(2016\)](#); [Li and Zhang \(2017\)](#); [Sun and Li \(2017\)](#); [Chen et al. \(2019\)](#) developed a series of regression models for a tensor-valued response, by imposing different structural assumptions on the resulting tensor regression coefficient. This line of works share a similar goal as ours; however, none of these existing methods can handle tensor response with partially observed entries. Moreover, none is able to pool information from the dynamic tensor data collected at adjacent time points. In our experiments, we show that, focusing only on the subset of completely observed tensor data, or ignoring the structural smoothness over time would both lead to considerable loss in estimation accuracy. Finally, there have been a number of related but rather different methods motivated by similar applications. Particularly, [Li et al. \(2013\)](#) considered an adaptive voxel-wise approach by modeling each entry of the dynamic tensor separately. We instead adopt a tensor regression approach by jointly modeling all the entries of the entire tensor. We later numerically compare our method with [Li et al. \(2013\)](#) and other solutions. [Xue and Qu \(2019\)](#) studied regression of multi-source data with missing values involving neuroimaging features. However, the images were summarized as vectors, instead of tensors, and were placed on the predictor side, while the response was a scalar. Similarly, [Feng et al. \(2019\)](#) developed a scalar-on-image regression model with missing image scans. By contrast, we consider a different regression problem, where the tensor is placed on the response side, and thus requires a different set of estimation and theoretical tools.

In this article, we develop a regression model with partially observed dynamic tensor as the response. We impose that the coefficient tensor to be both sparse and low-rank, which reduces the dimension of the parameter space, lessens the computational complexity, and improves the interpretability of the model. Furthermore, we impose a fusion structure along the temporal mode of the tensor coefficient, which helps pool the information from data

observed at adjacent time points. All these assumptions are scientifically plausible, and have been widely used in numerous applications including both neuroimaging analysis and digital advertising (Rabusseau and Kadri, 2016; Vounou et al., 2010; Zhou et al., 2013; Sun et al., 2017; Yin et al., 2015; Zhang et al., 2019). To handle the unobserved entries of the tensor response, we consider a loss function projected over the observed entries, which is then optimized under the low-rank, sparsity and fusion constraints. We develop an efficient non-convex alternating updating algorithm, and derive the finite-sample error bound of the actual estimator from each step of our optimization algorithm.

Unobserved entries in tensor response have introduced serious challenges, as the existing algorithms for estimating a sparse low-rank tensor and the technical tools for asymptotic analysis are only applicable to either a single partially observed tensor or a fully observed tensor. As a result, our proposal differs considerably in terms of estimation algorithm, regularity conditions, as well as theoretical properties, compared to the existing tensor completion or tensor response regression solutions (e.g., Jain and Oh, 2014; Sun and Li, 2017). For estimation, since the unobserved entries can occur at different locations for different tensors, the loss function projected over the observed entries takes a complex form. The traditional vector-wise updating algorithms (Jain and Oh, 2014; Sun and Li, 2017) are no longer applicable. Alternatively, we propose a new procedure that updates the low-rank components of the coefficient tensor in an element-wise fashion; see Step 1 of Algorithm 1 and equation (7) in Section 3. For regularity conditions, we add a  $\mu$ -mass condition to ensure that sufficient information are contained in the observed entries for tensor coefficient estimation; see Assumption 1. We also place a lower bound on the probability of the observation  $p$ , and discuss its relation with the sample size, tensor dimension, sparsity level and mass parameter  $\mu$ ; see Assumptions 2 and 6. Moreover, unlike the tensor response regression for complete data (Sun and Li, 2017), our condition on the initialization error now depends on the observation probability  $p$ ; see Assumptions 4 and 8. For theoretical properties, we show that both the converge rate of the algorithm and the statistical error of the estimator are affected by a factor of  $p^{-2}$ . These results characterize the loss at both the computational level and the statistical level when modeling with only partially observed tensor data. In summary, our proposal is far from an incremental extension from the complete case scenario, and involves a new set of strategies for estimation and theoretical analysis.

We adopt the following notations throughout the article. Let  $[d] = \{1, \dots, d\}$ , and let  $\circ$  denote the outer product. For a vector  $\mathbf{a} \in \mathbb{R}^d$ , let  $\|\mathbf{a}\|$  and  $\|\mathbf{a}\|_0$  denote its Euclidean norm and  $\ell_0$  norm, respectively. For a matrix  $\mathbf{A} \in \mathbb{R}^{d_1 \times d_2}$ , let  $\|\mathbf{A}\|$  denote its spectral norm. For a tensor  $\mathcal{A} \in \mathbb{R}^{d_1 \times \dots \times d_m}$ , let  $\mathcal{A}_{i_1, \dots, i_m}$  be its  $(i_1, \dots, i_m)$ th entry, and  $\mathcal{A}_{i_1, \dots, i_{j-1}, :, i_{j+1}, \dots, i_m} = (\mathcal{A}_{i_1, \dots, i_{j-1}, 1, i_{j+1}, \dots, i_m}, \dots, \mathcal{A}_{i_1, \dots, i_{j-1}, d_j, i_{j+1}, \dots, i_m})^\top \in \mathbb{R}^{d_j}$ . Define the tensor spectral norm as  $\|\mathcal{A}\| = \sup_{\|\mathbf{a}_1\|=\dots=\|\mathbf{a}_m\|=1} |\mathcal{A} \times_1 \mathbf{a}_1 \times_2 \dots \times_m \mathbf{a}_m|$ , and the tensor Frobenius norm as  $\|\mathcal{A}\|_F = \sqrt{\sum_{i_1, \dots, i_m} \mathcal{A}_{i_1, \dots, i_m}^2}$ . For a vector  $\mathbf{a} \in \mathbb{R}^{d_j}$ , define the  $j$ -mode tensor product as  $\mathcal{A} \times_j \mathbf{a} \in \mathbb{R}^{d_1 \times \dots \times d_{j-1} \times d_{j+1} \times \dots \times d_m}$ , such that  $(\mathcal{A} \times_j \mathbf{a})_{i_1, \dots, i_{j-1}, i_{j+1}, \dots, i_m} = \sum_{i_j=1}^{d_j} \mathcal{A}_{i_1, \dots, i_m} a_{i_j}$ . For vectors  $\mathbf{a}_j \in \mathbb{R}^{d_j}, j \in [m]$ , define the multilinear combination of the tensor entries as  $\mathcal{A} \times_1 \mathbf{a}_1 \times_2 \dots \times_m \mathbf{a}_m = \sum_{i_1 \in [d_1]} \dots \sum_{i_m \in [d_m]} a_{1, i_1} \dots a_{m, i_m} \mathcal{A}_{i_1, \dots, i_m}$ , where  $a_{j, i_j}$  is the  $i_j$ th entry of  $\mathbf{a}_j$ . Finally, for two sequences  $a_n, b_n$ , we say  $a_n = \mathcal{O}(b_n)$  if  $a_n \leq C b_n$  for some positive constant  $C$ .

The rest of the article is organized as follows. Section 2 introduces our regression model with partially observed dynamic tensor response. Section 3 develops the estimation algorithm. Section 4 investigates the theoretical properties. Section 5 presents the simulation results, and Section 6 illustrates with two real world datasets, a neuroimaging study and a digital advertising study. Supplementary Materials containing all technical proofs are available upon request.

## 2 Model

Suppose at each time point  $t$ , we collect an  $m$ th-order tensor  $\mathcal{Y}_t$  of dimension  $d_1 \times \dots \times d_m$ ,  $t \in [T]$ . We stack the collected tensors  $\mathcal{Y}_1, \dots, \mathcal{Y}_T$  together, and represent it as an  $(m+1)$ th-order tensor  $\mathcal{Y} \in \mathbb{R}^{d_1 \times \dots \times d_m \times T}$ . Correspondingly, the  $(m+1)$ th mode of  $\mathcal{Y}$  is referred as the temporal mode. Suppose there are totally  $n$  subjects in the study. For each subject  $i$ , we collect a dynamic tensor represented as  $\mathcal{Y}_i$ , along with a  $q$ -dimensional vector of covariates  $\mathbf{x}_i \in \mathbb{R}^q, i \in [n]$ . The response tensor  $\mathcal{Y}_i$  can be partially observed, and the missing patterns can vary from subject to subject. We consider the following regression model,

$$\mathcal{Y}_i = \mathcal{B}^* \times_{m+2} \mathbf{x}_i + \mathcal{E}_i, \quad (1)$$

where  $\mathcal{B}^* \in \mathbb{R}^{d_1 \times \dots \times d_m \times T \times q}$  is an  $(m+2)$ th-order coefficient tensor, and  $\mathcal{E}_i \in \mathbb{R}^{d_1 \times \dots \times d_m \times T}$  is an  $(m+1)$ th-order error tensor independent of  $\mathbf{x}_i$ . Without loss of generality, we assume the data are centered, and thus drop the intercept term in model (1). The coefficient tensor  $\mathcal{B}^*$

captures the relationship between the dynamic tensor response and the predictor, and is the main object of interest in our analysis. For instance,  $\mathcal{B}_{i_1, \dots, i_m, :, l}^* \in \mathbb{R}^T$  describes the effect of the  $l$ th covariate on the time-varying pattern of the  $(i_1, \dots, i_m)$ th entry of tensor  $\mathcal{Y}_t$ . Next, we impose three structures on  $\mathcal{B}^*$  to facilitate its analysis.

We first assume that  $\mathcal{B}^*$  admits a rank- $r$  CP decomposition structure, in that,

$$\mathcal{B}^* = \sum_{k \in [r]} w_k^* \beta_{k,1}^* \circ \dots \circ \beta_{k,m+2}^*, \quad (2)$$

where  $\beta_{k,j}^* \in \mathbb{S}^{d_j}$ ,  $\mathbb{S}^d = \{\mathbf{a} \in \mathbb{R}^d \mid \|\mathbf{a}\| = 1\}$ , and  $w_k^* > 0$ . The CP structure is one of the most common low-rank structures (Kolda and Bader, 2009), and is widely used in tensor data analysis (Zhou et al., 2013; Anandkumar et al., 2014; Jain and Oh, 2014; Yuan and Zhang, 2016, 2017; Zhang, 2019; Chen et al., 2019, among others). We next assume that  $\mathcal{B}^*$  is sparse, in that the decomposed components  $\beta_{k,j}^*$ 's are sparse. That is,  $\beta_{k,j}^* \in \mathcal{S}(d_j, s_j)$  for  $j \in [m+1], k \in [r]$ , where

$$\mathcal{S}(d, s) = \left\{ \beta \in \mathbb{R}^d \mid \sum_{l=1}^d 1_{(\beta_l \neq 0)} \leq s \right\} = \{ \beta \in \mathbb{R}^d \mid \|\beta\|_0 \leq s \}.$$

This assumption postulates that the covariates  $\mathbf{x}$ 's effects are concentrated on a subset of entries of  $\mathcal{B}^*$ , which enables us to identify most relevant regions in the dynamic tensor that are affected by the covariates. The sparsity assumption is again widely employed in numerous applications including neuroscience and online advertising (Bullmore and Sporns, 2009; Vounou et al., 2010; Sun et al., 2017). We further assume a fusion structure on the decomposed components  $\beta_{k,j}^*$  of  $\mathcal{B}^*$ . That is,  $\beta_{k,j}^* \in \mathcal{F}(d_j, f_j)$  for  $j \in [m+1], k \in [r]$ , where

$$\mathcal{F}(d, f) = \left\{ \beta \in \mathbb{R}^d \mid \sum_{l=2}^d 1_{(|\beta_l - \beta_{l-1}| \neq 0)} \leq f \right\} = \{ \beta \in \mathbb{R}^d \mid \|\mathbf{D}\beta\|_0 \leq f - 1 \},$$

and  $\mathbf{D} \in \mathbb{R}^{(d-1) \times d}$  with  $\mathbf{D}_{i,i} = -1$ ,  $\mathbf{D}_{i,i+1} = 1$  for  $i \in [d-1]$ , and other entries being zeros. This assumption encourages temporal smoothness and helps pool information from tensors observed at adjacent time points (Madrid-Padilla and Scott, 2017; Sun and Li, 2019). Putting the sparsity and fusion structures together, we have

$$\beta_{k,j}^* \in \mathcal{S}(d_j, s_j) \cap \mathcal{F}(d_j, f_j), \quad \text{for } j \in [m+1], k \in [r]. \quad (3)$$

We briefly comment that, since the dimension  $q$  of the covariates  $\mathbf{x}$  is relatively small in our motivating examples, we have chosen not to impose sparsity or fusion structure on the

component  $\beta_{k,m+2}^* \in \mathbb{R}^q$ , which is the last mode of the coefficient tensor  $\mathcal{B}^*$ . On the other hand, we can easily modify our method to incorporate any structure for  $\beta_{k,m+2}^*$ , or other structures for the decomposed components of  $\mathcal{B}^*$ . The extension is straightforward, and thus is not further pursued in this article.

A major challenge we face is that many entries of the dynamic tensor response  $\mathcal{Y}$  are unobserved. Let  $\Omega \subseteq [d_1] \times [d_2] \times \cdots \times [d_{m+1}]$  denote the set of indexes for the observed entries, and  $\Omega_i$  denote the set of indexes for the observed entries in  $\mathcal{Y}_i$ ,  $i \in [n]$ . We define a projection function  $\Pi_\Omega(\cdot)$  that projects the tensor onto the observed set  $\Omega$ , such that

$$[\Pi_\Omega(\mathcal{Y})]_{i_1, i_2, \dots, i_{m+1}} = \begin{cases} \mathcal{Y}_{i_1, i_2, \dots, i_{m+1}} & \text{if } (i_1, \dots, i_{m+1}) \in \Omega, \\ 0 & \text{otherwise.} \end{cases}$$

We then consider the following constrained optimization problem,

$$\begin{aligned} \min_{w_k, \beta_{k,j}} \quad & \frac{1}{n} \sum_{i=1}^n \left\| \Pi_{\Omega_i} \left( \mathcal{Y}_i - \sum_{k \in [r]} w_k (\beta_{k,m+2}^\top \mathbf{x}_i) \beta_{k,1} \circ \cdots \circ \beta_{k,m+1} \right) \right\|_F^2 \\ \text{subject to} \quad & \|\beta_{k,j}\|_2 = 1, j \in [m+2], \|\beta_{k,j}\|_0 \leq \tau_{s_j}, \|\mathbf{D}\beta_{k,j}\|_0 \leq \tau_{f_j}, j \in [m+1], k \in [r]. \end{aligned} \quad (4)$$

In this optimization, both sparsity and fusion structures are imposed through  $\ell_0$  penalties. Such non-convex penalties have been found effective in high-dimensional sparse models (Shen et al., 2012; Zhu et al., 2014) and fused sparse models (Rinaldo, 2009; Wang et al., 2016).

### 3 Estimation

The optimization problem in (4) is highly nontrivial, as it is a non-convex optimization with multiple constraints and a complex loss function due to the unobserved entries. We develop an alternating block updating algorithm to solve (4), and divide our procedure into multiple alternating steps. First, we solve an unconstrained weighted tensor completion problem, by updating  $\beta_{k,1}, \dots, \beta_{k,m+1}$ , given  $w_k$  and  $\beta_{k,m+2}$ , for  $k \in [r]$ . Since each response tensor is only partially observed and different tensors may have different missing patterns, the commonly used vector-wise updating approach in tensor analysis (Jain and Oh, 2014; Sun and Li, 2017) is no longer applicable. To address this issue, we propose a new element-wise approach to update the decomposed components of the low-rank coefficient tensor. Next, we define a series of operators and apply them to the unconstrained estimators obtained from the first

---

**Algorithm 1** Alternating block updating algorithm for (4)

---

- 1: **input:** the data  $\{(\mathbf{x}_i, \mathcal{Y}_i, \Omega_i), i = 1, \dots, n\}$ , the rank  $r$ , the sparsity parameter  $\tau_{s_j}$ , and the fusion parameter  $\tau_{f_j}$ ,  $j \in [m+1]$ .
  - 2: **initialization:** set  $w_k = 1$ , and randomly generate unit-norm vectors  $\beta_{k,1}, \dots, \beta_{k,m+2}$  from a standard normal distribution,  $k \in [r]$ .
  - 3: **repeat**
  - 4:   **for**  $j = 1$  to  $m+1$  **do**
  - 5:     step 1: obtain the unconstrained estimator  $\tilde{\beta}_{k,j}^{(t+1)}$ , given  $\hat{w}_k^{(t)}$ ,  $\hat{\beta}_{k,1}^{(t)}, \dots, \hat{\beta}_{k,j-1}^{(t)}$ ,  $\hat{\beta}_{k,j+1}^{(t)}, \dots, \hat{\beta}_{k,m+1}^{(t)}, \hat{\beta}_{k,m+2}^{(t)}$ , by solving (5); normalize  $\tilde{\beta}_{k,j}^{(t+1)}$ ,  $k \in [r]$ .
  - 6:     step 2: obtain the constrained estimator  $\hat{\beta}_{k,j}^{(t+1)}$ , by applying the **Truncatefuse** operator to  $\tilde{\beta}_{k,j}^{(t+1)}$ ; normalize  $\hat{\beta}_{k,j}^{(t+1)}$ ,  $k \in [r]$ .
  - 7:   **end for**
  - 8:   step 3: obtain  $\hat{w}_k^{(t+1)}$ , given  $\hat{\beta}_{k,1}^{(t+1)}, \dots, \hat{\beta}_{k,m+1}^{(t+1)}, \hat{\beta}_{k,m+2}^{(t)}$ , using (8),  $k \in [r]$ .
  - 9:   step 4: obtain  $\hat{\beta}_{k,m+2}^{(t+1)}$ , given  $\hat{w}_k^{(t+1)}, \hat{\beta}_{k,1}^{(t+1)}, \dots, \hat{\beta}_{k,m+1}^{(t+1)}$ , using (9),  $k \in [r]$ .
  - 10: **until** the stopping criterion is met.
  - 11: **output:**  $\hat{w}_k, \hat{\beta}_{k,1}, \dots, \hat{\beta}_{k,m+2}$ ,  $k \in [r]$ .
- 

step, so to incorporate the sparsity and fusion constraints on  $\beta_{k,1}, \dots, \beta_{k,m+1}$ . Finally, we update  $w_k$  and  $\beta_{k,m+2}$  in turn, both of which have closed-form solutions. We summarize our procedure in Algorithm 1, then discuss each step in detail.

In step 1, we solve an unconstrained weighted tensor completion problem,

$$\min_{\beta_{k,j}} \frac{1}{n} \sum_{i=1}^n \left\{ \alpha_{i,k}^{(t)} \right\}^2 \left\| \Pi_{\Omega_i} \left( \mathcal{R}_{i,k}^{(t)} - \hat{w}_k^{(t)} \hat{\beta}_{k,1}^{(t)} \circ \dots \circ \hat{\beta}_{k,j-1}^{(t)} \circ \beta_{k,j} \circ \hat{\beta}_{k,j+1}^{(t)} \circ \dots \circ \hat{\beta}_{k,m+1}^{(t)} \right) \right\|_F^2, \quad (5)$$

where  $\alpha_{i,k}^{(t)} = \beta_{k,m+2}^{(t)\top} \mathbf{x}_i$ , and  $\mathcal{R}_{i,k}^{(t)}$  is a residual term defined as,

$$\mathcal{R}_{i,k}^{(t)} = \left( \mathcal{Y}_i - \sum_{k' \neq k, k' \in [r]} \hat{w}_{k'}^{(t)} \alpha_{i,k'}^{(t)} \beta_{k',1}^{(t)} \circ \dots \circ \beta_{k',m+1}^{(t)} \right) / \alpha_{i,k}^{(t)}, \quad (6)$$

for  $i \in [n], k \in [r]$ . The optimization problem in (5) has a closed-form solution. To simplify the presentation, we give this explicit expression when  $m = 2$ . For the case of  $m \geq 3$ , the calculation is similar except involving more terms. Specifically, the  $l$ th entry of  $\tilde{\beta}_{k,3}^{(t+1)}$  is

$$\tilde{\beta}_{k,3,l}^{(t+1)} = \frac{\sum_{i=1}^n \left\{ \alpha_{i,k}^{(t)} \right\}^2 \sum_{l_1, l_2} \delta_{i,l_1, l_2, l} \mathcal{R}_{i,k,l_1, l_2, l}^{(t)} \hat{\beta}_{k,1, l_1}^{(t)} \hat{\beta}_{k,2, l_2}^{(t)}}{\sum_{i=1}^n \left\{ \alpha_{i,k}^{(t)} \right\}^2 \sum_{l_1, l_2} \hat{w}_k^{(t)} \delta_{i,l_1, l_2, l} \left\{ \hat{\beta}_{k,1, l_1}^{(t)} \right\}^2 \left\{ \hat{\beta}_{k,2, l_2}^{(t)} \right\}^2}, \quad (7)$$

where  $\delta_{i,l_1, l_2, l} = 1$  if  $(l_1, l_2, l) \in \Omega_i$ , and  $\delta_{i,l_1, l_2, l} = 0$  otherwise. Here  $\mathcal{R}_{i,k,l_1, l_2, l}^{(t)}$  refers to the  $(l_1, l_2, l)$ th entry of  $\mathcal{R}_{i,k}^{(t)}$ . The expressions for  $\tilde{\beta}_{k,1}^{(t+1)}$  and  $\tilde{\beta}_{k,2}^{(t+1)}$  can be derived similarly. We

remark that, (7) is the key difference between our estimation method and those for a single partially observed tensor (Jain and Oh, 2014), or a completely observed tensor (Sun and Li, 2017). Particularly, the observed entry indicator  $\delta_{i,l_1,l_2,l}$  appears in both the numerator and denominator, and  $\delta_{i,l_1,l_2,l}$  is different across different entries of  $\tilde{\beta}_{k,3}^{(t+1)}$ . Therefore,  $\tilde{\beta}_{k,3}^{(t+1)}$  needs to be updated in an element-wise fashion, as  $\delta_{i,l_1,l_2,l}$  could not be cancelled. After obtaining (7), we normalize  $\tilde{\beta}_{k,j}^{(t+1)}$  to ensure a unit norm.

In step 2, we apply the sparsity and fusion constraints to  $\tilde{\beta}_{k,j}^{(t+1)}$  obtained in the first step. Toward that goal, we define a truncation operator  $\text{Truncate}(\mathbf{a}, \tau_s)$ , and a fusion operator  $\text{Fuse}(\mathbf{a}, \tau_f)$ , for a vector  $\mathbf{a} \in \mathbb{R}^d$  and two integer-valued tuning parameters  $\tau_s$  and  $\tau_f$ , as,

$$[\text{Truncate}(\mathbf{a}, \tau_s)]_j = \begin{cases} a_j & \text{if } j \in \text{supp}(\mathbf{a}, \tau_s) \\ 0 & \text{otherwise} \end{cases}; \quad [\text{Fuse}(\mathbf{a}, \tau_f)]_j = \sum_{i=1}^{\tau_f} 1_{j \in \mathcal{C}_i} \frac{1}{|\mathcal{C}_i|} \sum_{l \in \mathcal{C}_i} a_l,$$

where  $\text{supp}(\mathbf{a}, \tau_s)$  refers to the indexes of  $s$  entries with the largest absolute values in  $\mathbf{a}$ , and  $\{\mathcal{C}_i\}_{i=1}^{\tau_f}$  are the fusion groups. This truncation operator ensures that the total number of non-zero entries in  $\mathbf{a}$  is bounded by  $\tau_s$ , and is commonly employed in non-convex sparse optimizations (Yuan and Zhang, 2013; Sun et al., 2017). The fusion groups  $\{\mathcal{C}_i\}_{i=1}^{\tau_f}$  are calculated as follows. First, the truncation operator is applied to  $\mathbf{D}\mathbf{a} \in \mathbb{R}^{d-1}$ . The resulting  $\text{Truncate}(\mathbf{D}\mathbf{a}, \tau_f - 1)$  has at most  $(f - 1)$  non-zero entries. Then the elements  $a_j$  and  $a_{j+1}$  are put into the same group if  $[\text{Truncate}(\mathbf{D}\mathbf{a}, \tau_f - 1)]_j = 0$ . This procedure in effect groups the elements in  $\mathbf{a}$  into  $\tau_f$  distinct groups, which we denote as  $\{\mathcal{C}_i\}_{i=1}^{\tau_f}$ . Elements in each of the  $\tau_f$  groups are then averaged to obtain the final result. Combining the two operators, we obtain the  $\text{Truncatefuse}(\mathbf{a}, \tau_s, \tau_f)$  operator as,

$$\text{Truncatefuse}(\mathbf{a}, \tau_s, \tau_f) = \text{Truncate}\{\text{Fuse}(\mathbf{a}, \tau_f), \tau_s\},$$

where  $\tau_s \leq d$  is the sparsity parameter, and  $\tau_f \leq d$  is the fusion parameter. For example, consider  $\mathbf{a} = (0.1, 0.2, 0.4, 0.5, 0.6)^\top$ ,  $\tau_s = 3$  and  $\tau_f = 2$ . Correspondingly,  $\mathbf{D}\mathbf{a} = (0.1, 0.2, 0.1, 0.1)^\top$ . We then have  $\text{Truncate}(\mathbf{D}\mathbf{a}, \tau_f - 1) = (0, 0.2, 0, 0)^\top$ . This in effect suggests that  $a_1, a_2$  belong to one group, and  $a_3, a_4, a_5$  belong to the other group. We then average the values of  $\mathbf{a}$  in each group, and obtain  $\text{Fuse}(\mathbf{a}, \tau_f) = (0.15, 0.15, 0.5, 0.5, 0.5)^\top$ . Lastly,  $\text{Truncatefuse}(\mathbf{a}, \tau_s, \tau_f) = \text{Truncate}\{\text{Fuse}(\mathbf{a}, \tau_f), \tau_s\} = \text{Truncate}\{(0.15, 0.15, 0.5, 0.5, 0.5)^\top, 3\} = (0, 0, 0.5, 0.5, 0.5)^\top$ . We apply the  $\text{Truncatefuse}$  operator to the unconstrained estimator  $\tilde{\beta}_{k,j}^{(t+1)}$  obtained from the first step, with the sparsity parameter  $\tau_{s_j}$  and the fusion

parameter  $\tau_{f_j}$ , and normalize the result to ensure a unit norm.

After iterating through the updates of  $\tilde{\beta}_{k,1}^{(t+1)}$  to  $\tilde{\beta}_{k,m+1}^{(t+1)}$  by steps 1 and 2, one may repeat this process multiple times until the estimates become stable. For presentation simplicity, we list only one round of updates in Algorithm 1.

In step 3, we update  $\hat{w}_k^{(t+1)}$ , given  $\hat{\beta}_{k,1}^{(t+1)}, \dots, \hat{\beta}_{k,m+1}^{(t+1)}, \hat{\beta}_{k,m+2}^{(t)}$ , which has a closed-form solution,

$$\hat{w}_k^{(t+1)} = \frac{\mathcal{R}^{(t+1)} \times_1 \hat{\beta}_{k,1}^{(t+1)} \times_2 \dots \times_{m+1} \hat{\beta}_{k,m+1}^{(t+1)}}{\sum_{i=1}^n \left\{ \alpha_{i,k}^{(t)} \right\}^2 \left\| \Pi_{\Omega_i} \left( \hat{\beta}_{k,1}^{(t+1)} \circ \dots \circ \hat{\beta}_{k,m+1}^{(t+1)} \right) \right\|_F^2}, \quad (8)$$

where  $\mathcal{R}^{(t+1)} = \sum_{i=1}^n \left\{ \alpha_{i,k}^{(t)} \right\}^2 \Pi_{\Omega_i} \left( \mathcal{R}_{i,k}^{(t+1)} \right)$ , and  $\mathcal{R}_{i,k}^{(t+1)}$  is as defined in (6) by replacing  $\hat{\beta}_{k,1}^{(t)}, \dots, \hat{\beta}_{k,m+1}^{(t)}$  with  $\hat{\beta}_{k,1}^{(t+1)}, \dots, \hat{\beta}_{k,m+1}^{(t+1)}$ .

In step 4, we update  $\hat{\beta}_{k,m+2}^{(t+1)}$ , given  $\hat{w}_k^{(t+1)}, \hat{\beta}_{k,1}^{(t+1)}, \dots, \hat{\beta}_{k,m+1}^{(t+1)}$ , which again has a closed-form solution. Write  $\tilde{\mathcal{R}}_{i,k}^{(t+1)} = \mathcal{Y}_i - \sum_{k' \neq k, k' \in [r]} w_{k'}^{(t+1)} \alpha_{i,k'}^{(t)} \beta_{k',1}^{(t+1)} \circ \dots \circ \beta_{k',m+1}^{(t+1)}$ , and  $\mathcal{A}_k^{(t+1)} = w_k^{(t+1)} \beta_{k,1}^{(t+1)} \circ \dots \circ \beta_{k,m+1}^{(t+1)}$ . Then we have,

$$\hat{\beta}_{k,m+2}^{(t+1)} = \left\{ \frac{1}{n} \sum_{i=1}^n \left\| \Pi_{\Omega_i} \left( \mathcal{A}_k^{(t+1)} \right) \right\|_F^2 \mathbf{x}_i \mathbf{x}_i^\top \right\}^{-1} n^{-1} \sum_{i=1}^n \left\langle \Pi_{\Omega_i} \left( \tilde{\mathcal{R}}_{i,k}^{(t+1)} \right), \Pi_{\Omega_i} \left( \mathcal{A}_k^{(t+1)} \right) \right\rangle \mathbf{x}_i, \quad (9)$$

where  $\langle \cdot, \cdot \rangle$  is the tensor inner product.

We iterate through the above steps until the estimates from two consecutive iterations are close enough; i.e.,

$$\max_{j \in [m+2], k \in [r]} \min \left\{ \left\| \hat{\beta}_{k,j}^{(t+1)} - \hat{\beta}_{k,j}^{(t)} \right\|, \left\| \hat{\beta}_{k,j}^{(t+1)} + \hat{\beta}_{k,j}^{(t)} \right\| \right\} \leq 10^{-4}.$$

The proposed Algorithm 1 involves a number of tuning parameters, including the rank  $r$ , the sparsity parameter  $\tau_{s_j}$ , and the fusion parameter  $\tau_{f_j}$ ,  $j \in [m+1]$ . We propose to tune the parameters by minimizing a BIC-type criterion,

$$2 \log \left\{ \frac{1}{n} \sum_{i=1}^n \left\| \Pi_{\Omega_i} \left( \mathcal{Y}_i - \hat{\mathcal{B}} \times_{m+2} \mathbf{x}_i \right) \right\|_F^2 \right\} + \frac{\log \left( n \prod_{j=1}^{m+1} d_j \right)}{n \prod_{j=1}^{m+1} d_j} \times \text{df}, \quad (10)$$

where the total degrees of freedom df is the total number of unique nonzero entries of  $\beta_{k,j}$ . The criterion in (10) naturally balances the model fitting and model complexity. Similar BIC-type criteria have been used in tensor data analysis (Zhou et al., 2013; Wang et al., 2015a; Sun and Li, 2017). To further speed up the computation, we tune the three sets of parameters  $r$ ,  $\tau_{s_j}$  and  $\tau_{f_j}$  sequentially.

## 4 Theory

We next derive the non-asymptotic error bound of the actual estimator obtained from Algorithm 1. We first develop the theory for the case of rank  $r = 1$ , because this case has clearly captured the roles of various parameters, including the sample size, tensor dimension, and proportion of the observed entries, on both the computational and statistical errors. We then generalize to the case of rank  $r > 1$ . We comment that, our theoretical analysis is highly nontrivial, and is considerably different from Sun and Li (2017, 2019), due to the involvement of the unobserved entries. We discuss in detail the effect of missing entries on both the regularity conditions and the theoretical properties.

We first introduce some basic model assumptions common for both  $r = 1$  and  $r > 1$ .

**Assumption 1.** *Assume the following conditions hold.*

- (i) *The predictor  $\mathbf{x}_i$  satisfies that  $\|\mathbf{x}_i\| \leq c_1$ ,  $n^{-1} \sum_{i=1}^n \|\mathbf{x}_i \mathbf{x}_i^\top\|_2 \leq c_2$ ,  $i \in [n]$ , and  $1/c_0 < \lambda_{\min} \leq \lambda_{\max} < c_0$ , where  $\lambda_{\min}, \lambda_{\max}$  are the minimum and maximum eigenvalues of the sample covariance matrix  $\Sigma = n^{-1} \sum_{i=1}^n \mathbf{x}_i \mathbf{x}_i^\top$ , respectively, and  $c_0, c_1, c_2$  are some positive constants.*
- (ii) *The true tensor coefficient  $\mathcal{B}^*$  in (1) satisfies the CP decomposition (2) with sparsity and fusion constraints (3), and the decomposition is unique up to a permutation. Moreover,  $\|\mathcal{B}^*\| \leq c_3 w_{\max}^*$ , and  $w_{\min}^* > 1/c_4$  where  $w_{\max}^* = \max_k \{w_k^*\}$ ,  $w_{\min}^* = \min_k \{w_k^*\}$ , and  $c_3, c_4$  are some positive constants.*
- (iii) *The decomposed component  $\beta_{k,j}^*$  is a  $\mu$ -mass unit vector, in that  $\max_{l \in d_j} |\beta_{k,j,l}^*| \leq \mu/\sqrt{d}$ ,  $k \in [r]$ ,  $j \in [m+1]$ , where  $d = \max\{d_1, \dots, d_{m+1}\}$ .*
- (iv) *The entries of the error tensor  $\mathcal{E}_i \in \mathbb{R}^{d_1 \times d_2 \times d_3}$  are i.i.d. standard normally distributed.*
- (v) *The entries of the dynamic tensor response  $\mathcal{Y}_i$  are observed independently with an equal probability  $p \in (0, 1]$ .*

We make some remarks about these conditions. Assumption 1(i) is placed on the design matrix, which is mild and can be easily verified when  $\mathbf{x}_i$  is of a fixed dimension. Assumption 1(ii) is about the key structures we impose on the coefficient tensor  $\mathcal{B}^*$ . It also ensures the

identifiability of the decomposition of  $\mathcal{B}^*$ , which is always imposed in CP decomposition based tensor analysis (Zhou et al., 2013; Sun and Li, 2017; Chen et al., 2019). The condition on  $w_{\min}^*$  is mild and is satisfied as long as the signal level does not degenerate. It is also weaker than Sun and Li (2019) who required  $w_{\min}^*$  to be an increasing function of the dimension. Assumption 1(iii) is to ensure that the mass of the tensor would not concentrate on only a few entries. In that extreme case, randomly observed entries of the tensor response may not contain enough information to recover  $\mathcal{B}^*$ . Note that, since  $\beta_{k,j}^*$  is a vector of unit length, a relatively small  $\mu$  implies that the nonzero entries in  $\beta_{k,j}^*$  would be more uniformly distributed. This condition has been commonly imposed in the tensor completion literature for the same purpose (Jain and Oh, 2014). Assumption 1(iv) assumes the error terms are normally distributed, so that the explicit form of the statistical error can be derived. This assumption is again fairly common in theoretical analysis of tensor models (Anandkumar et al., 2017; Raskutti and Yuan, 2019). Finally, Assumption 1(v) specifies the mechanism of how each entry of the tensor response is observed, which is assumed to be independent of each other and have an equal observation probability. We recognize that this is a relatively simple mechanism. It may not always hold in real applications, as the actual observation patterns of the tensor data can depend on multiple factors, and may not be independent for different entries. We impose this condition for our theoretical analysis, even though our estimation algorithm does not require it. In the tensor completion literature, this mechanism has been commonly assumed (Jain and Oh, 2014; Yuan and Zhang, 2016, 2017; Xia and Yuan, 2017). We have chosen to impose this assumption because the theory of supervised tensor learning even for this simple mechanism remains unclear, and is far from trivial. We feel a rigorous theoretical analysis for this mechanism itself deserves a full investigation. We leave the study under a more general observation mechanism as future research.

## 4.1 Theory with $r = 1$

To ease the notation and simplify the presentation, we focus primarily on the case with a third-order tensor response, i.e.,  $m = 2$ . This however does not lose generality, as all our results can be extended to the case of  $m > 2$  in a straightforward fashion. Next, we introduce some additional regularity conditions. Let  $s_j$  denote the number of nonzero entries in  $\beta_{k,j}^*$ ,  $j \in [m + 1]$ , and  $s = \max_j \{s_j\}$ .

**Assumption 2.** Assume the observation probability  $p$  satisfies that,

$$p \geq \max \left\{ \frac{c_5 s_1 s_2 s_3 (\log d) \mu^4}{n^{1/3} d^2}, \frac{c_6 \mu^6 (\log d)^4}{d^{3/2}} \right\}.$$

where  $c_5, c_6$  are some positive constants.

Due to Assumption 1(v), the observation probability  $p$  also reflects the proportion of the observed entries of the tensor response. Assumption 2 places a lower bound on this proportion to ensure a good recovery of the tensor coefficient. This bound depends on the sample size  $n$ , maximum dimension  $d$ , mass parameter  $\mu$ , and true sparsity parameters  $s_1, s_2, s_3$ . This lower bound decreases as the sample size increases. It also decreases when the maximum dimension  $d$  increases, which reveals the blessing of dimensionality phenomenon often observed in tensor analysis (Jain and Oh, 2014; Sun et al., 2015). On the other hand, this lower bound increases as the mass parameter  $\mu$  increases. This is because when  $\mu$  increases, the mass of the tensor may become more likely to concentrate on a few entries, and thus the entries need to be observed with a larger probability to ensure the estimation accuracy. We also comment that our bound on  $p$  is very different from that in the tensor completion literature (Jain and Oh, 2014; Yuan and Zhang, 2016, 2017; Xia and Yuan, 2017), all of which only considered a single tensor. By comparison, we tackle a collection of  $n$  tensors, and consequently, our bound is a function of the number of tensors  $n$  under consideration.

**Assumption 3.** Assume the sparsity and fusion parameters satisfy that  $\tau_{s_j} \geq s_j, \tau_{s_j} = \mathcal{O}(s_j)$ , and  $\tau_{f_j} \geq f_j$ . Moreover, define the minimal gap,  $\Delta^* = \min_{1 \leq s \leq d_j, \beta_{1,j,s}^* \neq \beta_{1,j,s-1}^*, j \in [3]} |\beta_{1,j,s}^* - \beta_{1,j,s-1}^*|$ . Assume that, for some positive constants  $C_1, C_2$ ,

$$\Delta^* > \frac{C_1 \sqrt{s}}{n^{1/3}} + \frac{C_2}{w_1^*} \sqrt{\frac{s_1 s_2 s_3 \log(d_1 d_2 d_3)}{n}}.$$

The condition for the sparsity parameter ensures that the truly nonzero elements would not be shrunk to zero. Similar conditions have been imposed in truncated sparse models (Yuan and Zhang, 2013; Wang et al., 2015b; Sun et al., 2017; Tan et al., 2018). The conditions for the fusion parameter and the minimum gap ensure that the fused estimator would not incorrectly merge two distinct groups of entries in the true parameter. Such conditions are common in sparse and fused regression models (Tibshirani et al., 2005; Rinaldo, 2009). Moreover, in the lower bound for  $\Delta^*$ , the term  $C_1 \sqrt{s}/n^{1/3}$  appears due to the unobserved entries and the techniques we use in our theoretical analysis.

**Assumption 4.** Define the initialization error,  $\epsilon = \max \left\{ |\widehat{w}_1^{(0)} - w_1^*|, \max_j \|\widehat{\beta}_{1,j}^{(0)} - \beta_{1,j}^*\|_2 \right\}$ . Assume that,

$$\epsilon < \min \left\{ \frac{(1-C)^2 p^2 \lambda_{\min}^2}{12\sqrt{10} c_2 (3+c_4) \lambda_{\max}}, \frac{w_1^*}{2}, \frac{1}{2} \right\},$$

where  $0 < C < 1$  is a positive constant, and  $c_2, c_4$  are the same constants in Assumption 1.

This assumption is placed on the initialization error of Algorithm 1. It requires that the initial values are reasonably close to the true parameters. Comparing this condition to the initialization condition of Sun and Li (2017) for tensor response regression with completely observed data, the key difference is that the upper bound for the initialization error now depends on the observation probability  $p$ . By Assumption 1(i),  $\lambda_{\min}$  and  $\lambda_{\max}$  are bounded. When  $p$  is fixed, Assumption 4 indicates a constant bound for the initialization error, which has been considered in non-convex optimizations (Anandkumar et al., 2014; Balakrishnan et al., 2017). When  $p$  goes to zero, the error bound on  $\epsilon$  becomes tighter, which is consistent with the condition considered in the tensor completion literature (Jain and Oh, 2014; Yuan and Zhang, 2016, 2017; Xia and Yuan, 2017).

**Assumption 5.** Assume the sample size  $n$  satisfies that, for some positive constant  $c_7, c_8$

$$n \geq \max \left\{ \frac{c_7 d s_1 s_2 s_3 \log(d_1 d_2 d_3)}{w_1^{*2}}, c_8 (sd)^{3/2} \right\}.$$

We now state the main theory for the estimator of Algorithm 1 when  $r = 1$ .

**Theorem 1.** Suppose Assumptions 1, 2, 3, 4 and 5 hold. When the tensor rank  $r = 1$ , the estimator from the  $t$ -th iteration of Algorithm 1 satisfies that, with a high probability,

$$\begin{aligned} & \max \left[ |\widehat{w}_1^{(t)} - w_1^*|, \max_j \left\{ \|\widehat{\beta}_{1,j}^{(t)} - \beta_{1,j}^*\|_2 \right\} \right] \\ & \leq \underbrace{\kappa^t \epsilon}_{\text{computational error}} + \underbrace{\frac{1}{1-\kappa} \max \left\{ \frac{C_1 \sqrt{s}}{n^{1/3}}, \frac{C_2}{p^2 w_1^*} \sqrt{\frac{s_1 s_2 s_3 \log(d_1 d_2 d_3)}{n}} \right\}}_{\text{statistical error}}, \end{aligned}$$

where  $\kappa = \{12\sqrt{10}c_2(3+c_4)\lambda_{\max}\epsilon\} / \{(1-C)^2\lambda_{\min}^2 p^2\} < 1$ , and is the positive contraction coefficient, and the constants  $C_1 = 32\sqrt{10}C_0C/\lambda_{\min}$ ,  $C_2 = 8\sqrt{10}\tilde{C}C_0^3/\lambda_{\min} + 3\tilde{C}C_0^3\sqrt{q}/\{(1-C)^2\lambda_{\min}\}$ . Here  $c_2, c_4, C$  are the same constants defined in Assumptions 1 and 4,  $C_0 > 1$  and  $\tilde{C}$  are some positive constants, and  $q$  is fixed under Assumption 1(i).

The non-asymptotic error bound in Theorem 1 can be decomposed as the sum of a computational error and a statistical error. The former is related to the optimization procedure, while the latter is related to the statistical model. The contraction coefficient  $\kappa$  is a function of the observation probability  $p$  when other parameters are fixed. When  $p$  increases, i.e., when we observe more entries in the response tensor,  $\kappa$  decreases. The computational error decreases with a decreasing  $\kappa$ , and as such the algorithm is to converge faster with an increasing  $p$ . Meanwhile, the statistical error decreases with a decreasing  $\kappa$ , an increasing  $p$ , an increasing signal strength as reflected by  $w_1^*$ , and an increasing sample size  $n$ .

We observe that, both the converge rate of the algorithm and the statistical error of the model are affected by a factor of  $p^{-2}$ . This result characterizes the loss when modeling with partially observed tensor response, both at the computational level and the statistical level. This explicit characterization, to our best knowledge, is the first result of this kind in the literature. Furthermore, due to the unobserved entries and the techniques we use in our theoretical analysis, the statistical error includes an additional term  $C_1\sqrt{s}/n^{1/3}$ . Such a term does not show up when the response tensor is completely observed as in Sun and Li (2017). Actually, one of the key challenges of our theoretical analysis is the complicated form of the element-wise estimator  $\tilde{\beta}_{k,3}$  in (7) and its normalized version  $\tilde{\beta}_{k,3}/\|\tilde{\beta}_{k,3}\|$ . Consequently, one cannot directly characterize the distance between  $\tilde{\beta}_{k,3}/\|\tilde{\beta}_{k,3}\|$  and  $\beta_{k,3}^*$  with a simple analytical form. To overcome this challenge, a crucial and novel component of our theoretical analysis is to construct a new intermediate quantity  $\check{\beta}_{k,3}$ , whose entries share the same numerator but a different denominator as  $\tilde{\beta}_{k,3}$ . We then resort to an inequality between  $\check{\beta}_{k,3}/\|\check{\beta}_{k,3}\|$  and  $\tilde{\beta}_{k,3}/\|\tilde{\beta}_{k,3}\|$  to characterize the error of  $\tilde{\beta}_{k,3}/\|\tilde{\beta}_{k,3}\|$ . This is quite different from Sun and Li (2017), where one can directly characterize the error of  $\tilde{\beta}_{k,3}/\|\tilde{\beta}_{k,3}\|$  in a simple analytical form when all the entries of the tensor response are completely observed.

We also briefly comment that, the error bound in Theorem 1 provides a theoretical termination condition for Algorithm 1. When the number of iterations  $t$  exceeds

$$O\left(\log_{1/\kappa}\left[\frac{(1-\kappa)\epsilon}{\max\left\{\frac{C_1\sqrt{s}}{n^{1/3}}, \frac{C_2}{p^2w_1^*}\sqrt{\frac{s_1s_2s_3\log(d_1d_2d_3)}{n}}\right\}}\right]\right),$$

then the computational error is to be dominated by the statistical error, and the estimator falls within the statistical precision of the true parameters.

## 4.2 Theory with $r > 1$

Next, we extend our theory to the general rank  $r > 1$ . Due to the interplay among different decomposed components  $\beta_{k,j}$ , the general rank case requires some modifications of the regularity conditions compared to the rank one case.

**Assumption 6.** Assume the observation probability  $p$  satisfies that

$$p \geq \max \left\{ \frac{c_5 s_1 s_2 s_3 \mu^4 w_{\max}^* \log d}{n^{1/3} d^2 w_{\min}^*}, \frac{c_6 \mu^4 (\log d)^4}{d^{3/2}}, \frac{c_9 (\log d) \mu^4 (w_{\max}^*)^2 r}{w_{\min}^* n^{1/3} d^2} \right\},$$

where  $c_5, c_6$  are constants in Assumption 2, and  $c_9$  is some positive constant.

For the general rank case, the lower bound on the observation probability  $p$  depends on the rank  $r$ . Particularly, this lower bound increases with an increasing rank  $r$ , which suggests that more observations are needed if the rank of the coefficient tensor increases.

**Assumption 7.** Assume the sparsity and fusion parameters satisfy that  $\tau_{s_j} \geq s_j, \tau_{s_j} = \mathcal{O}(s_j)$ , and  $\tau_{f_j} \geq f_j$ . Moreover, define the minimal gap  $\Delta^* = \min_{1 < s \leq d_j, \beta_{k,j,s}^* \neq \beta_{k,j,s-1}^*, j \in [3], k \in [r], |\beta_{k,j,s}^* - \beta_{k,j,s-1}^*|}$ . Assume that, for some positive constants  $C_3, C_4$ ,

$$\Delta^* > \frac{C_3 \sqrt{s}}{n^{1/3}} + \frac{C_4}{w_{\min}^*} \sqrt{\frac{s_1 s_2 s_3 \log(d_1 d_2 d_3)}{n}}.$$

This assumption is similar to Assumption 3, and it reduces to Assumption 3 when  $r = 1$ .

**Assumption 8.** Assume the initial error  $\epsilon$  satisfies that,

$$\epsilon < \min \left\{ \frac{(1-C)^2 \lambda_{\min}^2 w_{\min}^* p^2}{12\sqrt{10}(8c_1 c_3 + \lambda_{\max})c_2(c_4 + 3)w_{\max}^* r} - 12(r-1)\xi, \frac{1}{9+c_4}, \frac{1}{2}, \frac{w_{\min}^*}{2} \right\},$$

where  $c_1, c_2, c_3, c_4$  are constants as defined in Assumption 1,  $0 < C < 1$  is some constant, and  $\xi$  is the incoherence parameter defined as,

$$\xi = \max_{j=1,2,3} \max_{k \neq k'} |\langle \beta_{k,j}^*, \beta_{k',j}^* \rangle|.$$

For the general rank case, we need to control the correlations between the decomposed components across different ranks. The incoherence parameter  $\xi$  is defined to quantify such correlations. It is seen that the initial error hinges on both the rank  $r$  and the incoherence measure  $\xi$ . The error bound on  $\epsilon$  becomes tighter when  $r$  or  $\xi$  increases, as in such cases the tensor recovery problem becomes more challenging. It is also noteworthy that, even when  $r = 1$  and  $\xi = 0$ , this condition is still stronger than Assumption 4. This is due to a different technique required in the theoretical analysis of the general rank case.

**Assumption 9.** Assume the sample size  $n$  satisfies that,

$$n \geq \max \left\{ \frac{c_7 d s_1 s_2 s_3 \log(d_1 d_2 d_3)}{w_{\min}^*}, c_8 (sd)^{3/2} \right\},$$

where  $c_7$  and  $c_8$  are positive constants as defined in Assumption 5.

This assumption is similar to Assumption 5, and it reduces to Assumption 5 when  $r = 1$ .

We next state the main theory for the estimator of Algorithm 1 when  $r > 1$ .

**Theorem 2.** Suppose Assumptions 1, 6, 7, 8 and 9 hold. For a general rank  $r$ , the estimator from the  $t$ -th iteration of Algorithm 1 satisfies that, with a high probability,

$$\begin{aligned} & \max \left[ \max_k |\widehat{w}_k^{(t)} - w_k^*|, \max_{k,j} \left\{ \|\widehat{\beta}_{k,j}^{(t)} - \beta_{k,j}^*\|_2 \right\} \right] \\ & \leq \underbrace{\widetilde{\kappa}^t \epsilon}_{\text{computational error}} + \underbrace{\frac{1}{1 - \widetilde{\kappa}} \max \left\{ \frac{C_3 \sqrt{s}}{n^{1/3}}, \frac{C_4}{p^2 w_{\min}^*} \sqrt{\frac{s_1 s_2 s_3 \log(d_1 d_2 d_3)}{n}} \right\}}_{\text{statistical error}}. \end{aligned}$$

where  $\widetilde{\kappa} = \{12\sqrt{10}c_1c_2(c_4 + 3)rw_{\max}^*\} \{(\lambda_{\max}/c_1 + 8c_3)\epsilon + 12(r - 1)\xi\} / \{(1 - C)^2\lambda_{\min}^2 p^2 w_{\min}^*\} < 1$ , and is the positive contraction coefficient, and the constants  $C_3 = 40\sqrt{10}C_0C/(\lambda_{\min})$  and  $C_4 = 8\sqrt{10}\widetilde{C}C_0^3/\lambda_{\min} + 3\widetilde{C}C_0^3\sqrt{q}/\{(1 - C)^2\lambda_{\min}\}$ .

When  $r = 1$ , the contraction coefficient  $\widetilde{\kappa}$  reduces to  $\kappa$  in Theorem 1 up to a constant. When  $r > 1$  and all other parameters are fixed,  $\widetilde{\kappa}$  is larger than  $\kappa$ , which indicates that the algorithm has a lower convergence rate for the general rank than the rank one case. Moreover,  $\widetilde{\kappa}$  increases with an increasing rank  $r$  and incoherence parameter  $\xi$ . This agrees with the expectation that, as the tensor recovery problem becomes more challenging, the algorithm has a slower convergence rate. It is also seen that, for the general rank case, the converge rate of the algorithm and the statistical error of the model are affected by a factor of  $p^{-2}$ , the same phenomenon as the rank one case.

## 5 Simulations

We carry out simulations to investigate the finite-sample performance of our proposed method. For easy reference, we call our method Partially ObServed dynamic Tensor rEsponse Regression (POSTER). We also compare with some alternative solutions. One competing

method is the multiscale adaptive generalized estimating equations method (**MAGEE**) proposed by Li et al. (2013), which integrated a voxel-wise approach with generalized estimating equations for adaptive analysis of dynamic tensor imaging data. Another competing method is the sparse tensor response regression method (**STORE**) proposed by Sun and Li (2017), which considered a sparse tensor response regression model but did not incorporate fusion type smoothness constraint and can only handle completely observed data. In our analysis, **STORE** is applied to the complete samples only. Moreover, to examine the effect of utilizing the partially observed samples, and of incorporation of structural smoothness over time, we also compare to our own method but only applied to the completely observed samples, or without fusion constraint, which serve as two benchmarks.

We consider two patterns for the unobserved entries, block missing in Section 5.1 and random missing in Section 5.2. Both patterns are common in real data applications. For instance, in our neuroimaging example, individual subjects would miss some scheduled biannual scans, and as a result, the entire tensor images are unobserved, and the missing pattern is more likely a block missing. In our digital advertising example, on the other hand, some users may randomly react to only a subset of advertisements on certain days, and the missing pattern is closer to a random missing. Finally, in Section 5.3, we consider a model used in Li et al. (2013). The data generation does not comply with our proposed model, and we examine the performance of our method under model misspecification.

To evaluate the estimation accuracy, we report the estimation error of the coefficient tensor  $\mathcal{B}$  measured by  $\|\hat{\mathcal{B}} - \mathcal{B}\|_F$ , and the estimation error of the decomposed components  $\hat{\beta}_{k,j}$  measured by  $\max_{k,j} \min\{\|\hat{\beta}_{k,j} - \beta_{k,j}\|, \|\hat{\beta}_{k,j} + \beta_{k,j}\|\}$ . To evaluate the variable selection accuracy, we compute the true positive rate as the mean of  $\text{TPR}_j$ , and the false positive rate as the mean of  $\text{FPR}_j$ , where  $\text{TPR}_j = K^{-1} \sum_{k=1}^K \sum_l 1(\beta_{k,j,l} \neq 0, \hat{\beta}_{k,j,l} \neq 0) / \sum_l 1(\beta_{k,j,l} \neq 0)$  is the true positive rate of the estimator in mode  $j$ , and  $\text{FPR}_j = K^{-1} \sum_{k=1}^K \sum_l 1(\beta_{k,j,l} = 0, \hat{\beta}_{k,j,l} \neq 0) / \sum_l 1(\beta_{k,j,l} = 0)$  is the false positive rate of the estimator in mode  $j$ .

## 5.1 Block missing

In the first example, we simulate a fourth-order tensor response  $\mathcal{Y}_i \in \mathbb{R}^{d_1 \times d_2 \times d_3 \times T}$ , where the fourth mode corresponds to the time dimension, and there are blocks of tensor entries missing along the time mode. More specifically, we generate the coefficient tensor  $\mathcal{B} \in \mathbb{R}^{d_1 \times d_2 \times d_3 \times T \times q}$

as  $\mathcal{B} = \sum_{k \in [r]} w_k \beta_{k,1} \circ \beta_{k,2} \circ \beta_{k,3} \circ \beta_{k,4} \circ \beta_{k,5}$ , where  $d_1 = d_2 = d_3 = 32, T = 5, q = 5$ , and the true rank  $r = 2$ . We generate the entries of  $\beta_{k,j}, j \in [4]$  as i.i.d. standard normal. We then apply the **Truncatefuse** operator on  $\beta_{k,j}, j \in [3]$ , with the true sparsity and fusion parameters  $(s_j, f_j), j \in [3]$ , and apply the **Fuse** operator to  $\beta_{k,4}$  with the true fusion parameter  $f_4$ . We set the true sparsity parameters  $s_j = s_0 \times d_j, j \in [3]$  with  $s_0 = 0.7$ , and set the true fusion parameters  $f_j = f_0 \times d_j, j \in [4]$ , with  $f_0 \in \{0.3, 0.7\}$ . A smaller  $f$  implies a smaller number of fusion groups in  $\beta_{k,j}$ . We set  $\beta_{k,5} = (1, \dots, 1)^\top$ , a vector of all ones. We then normalize each vector to have a unit norm. We set the weight  $w_k \in \{30, 40\}$ , with a larger weight indicating a stronger signal. Next, we generate the  $q$ -dimensional predictor vector  $\mathbf{x}_i$  whose entries are i.i.d. Bernoulli with probability 0.5, and the error tensor  $\mathcal{E}_i$ , whose entries are i.i.d. standard normal. Finally, we generate the response tensor  $\mathcal{Y}_i$  following model (1). We set the blocks of entries of  $\mathcal{Y}_i$  along the fourth mode randomly missing. Among all  $n$  subjects, we set the proportion of subjects with missing values  $m_n \in \{0.8, 0.9\}$ , and for each subject with missing values, we set the proportion of missing blocks along the time mode as  $m_t \in \{0.4, 0.6\}$ . For example,  $n = 100, m_n = 0.8$  and  $m_t = 0.4$  means there are 80 subjects out of 100 having partially observed tensors, and for each of those 80 subjects, the tensor observations at 2 out of 5 time points are missing.

Table 1 reports the average criteria based on 30 data replications with  $m_n = 0.8$ . The results with  $m_n = 0.9$  are similar qualitatively and are reported in Section ?? of the Appendix. Since the method **MAGEE** of Li et al. (2013) does not decompose the coefficient tensor and does not carry out variable selection, the corresponding criteria of  $\beta_{k,j}$  and selection are reported as NA. From this table, it is clearly seen that our proposed method outperforms all other competing methods in terms of both estimation accuracy and variable selection accuracy. In addition, the finite-sample performance of our method agrees with the theoretical findings.

The computational time of our method scales linearly with the sample size and tensor dimension. As an example, consider the simulation setup with  $m_n = 0.8, m_t = 0.4, w_k = 30$ , and  $f_0 = 0.3$ . When we fix  $d_1 = 32$  and other parameters, the average computational time of our method was 302.6, 535.1, 896.7 seconds for the sample size  $n = 100, 200, 300$ , respectively. When we fix  $n = 100$  and other parameters, the average computational time of our method was 108.8, 236.3, 302.0 seconds for the tensor dimension  $d_1 = 10, 20, 32$ , respectively. All simulations were run on a personal computer with a 3.2 GHz Intel Core i5 processor.

Table 1: Simulation example with block missing, for varying missing proportions  $m_n, m_t$ , signal strength  $w_k$ , and fusion setting  $f_0$ . Reported are the average estimation errors of  $\mathcal{B}$  and  $\beta_{k,j}$ , and the true and false positive rates of selection based on 30 data replications (the standard errors in the parentheses). Five methods are compared: STORE of Sun and Li (2017), MAGEE of Li et al. (2013), our method applied to the complete data only (Complete), our method without the fusion constraint (No-fusion), and our proposed method (POSTER).

$(m_n, m_t)$	$w_k$	$f_0$	method	Error of $\mathcal{B}$	Error of $\beta_{k,j}$	TPR	FPR
(0.8, 0.4)	30	0.3	STORE	0.586 (0.055)	0.992 (0.109)	0.879 (0.016)	0.369 (0.035)
			MAGEE	1.397 (0.005)	NA	NA	NA
			Complete	0.555 (0.071)	0.898 (0.120)	0.852 (0.025)	0.269 (0.041)
			No-fusion	0.117 (0.005)	0.102 (0.007)	1.000 (0.000)	0.120 (0.000)
			POSTER	0.078 (0.027)	0.076 (0.007)	1.000 (0.000)	0.020 (0.001)
		0.7	STORE	0.574 (0.063)	0.905 (0.113)	0.878 (0.019)	0.343 (0.043)
			MAGEE	1.411 (0.003)	NA	NA	NA
			Complete	0.524 (0.064)	0.857 (0.118)	0.882 (0.021)	0.312 (0.045)
			No-fusion	0.113 (0.005)	0.100 (0.007)	1.000 (0.000)	0.072 (0.000)
			POSTER	0.101 (0.005)	0.088 (0.007)	1.000 (0.000)	0.055 (0.003)
	40	0.3	STORE	0.287 (0.055)	0.402 (0.104)	0.957 (0.013)	0.212 (0.028)
			MAGEE	1.233 (0.002)	NA	NA	NA
			Complete	0.222 (0.054)	0.327 (0.100)	0.961 (0.016)	0.094 (0.029)
			No-fusion	0.105 (0.005)	0.099 (0.007)	1.000 (0.000)	0.120 (0.000)
			POSTER	0.071 (0.005)	0.075 (0.007)	1.000 (0.000)	0.020 (0.003)
		0.7	STORE	0.228 (0.052)	0.281 (0.090)	1.000 (0.000)	0.056 (0.003)
			MAGEE	1.250 (0.002)	NA	NA	NA
			Complete	0.243 (0.059)	0.321 (0.098)	0.965 (0.015)	0.153 (0.035)
(0.8, 0.6)	30	0.3	STORE	0.586 (0.055)	0.992 (0.109)	0.879 (0.016)	0.369 (0.035)
			MAGEE	1.515 (0.004)	NA	NA	NA
			Complete	0.555 (0.071)	0.898 (0.120)	0.852 (0.025)	0.269 (0.041)
			No-fusion	0.155 (0.007)	0.139 (0.008)	1.000 (0.000)	0.121 (0.001)
			POSTER	0.106 (0.006)	0.115 (0.009)	1.000 (0.000)	0.020 (0.003)
		0.7	STORE	0.593 (0.062)	0.948 (0.111)	1.000 (0.000)	0.074 (0.020)
			MAGEE	1.528 (0.004)	NA	NA	NA
			Complete	0.524 (0.064)	0.857 (0.118)	0.875 (0.019)	0.370 (0.047)
			No-fusion	0.156 (0.007)	0.151 (0.010)	0.885 (0.021)	0.328 (0.060)
			POSTER	0.143 (0.008)	0.139 (0.010)	1.000 (0.000)	0.000 (0.000)
	40	0.3	STORE	0.287 (0.055)	0.402 (0.104)	0.957 (0.013)	0.212 (0.028)
			MAGEE	1.310 (0.003)	NA	NA	NA
			Complete	0.222 (0.054)	0.327 (0.100)	0.961 (0.016)	0.094 (0.029)
			No-fusion	0.144 (0.007)	0.137 (0.008)	1.000 (0.000)	0.120 (0.000)
			POSTER	0.100 (0.006)	0.114 (0.009)	1.000 (0.000)	0.020 (0.003)
		0.7	STORE	0.228 (0.052)	0.281 (0.090)	1.000 (0.000)	0.054 (0.003)
			MAGEE	1.325 (0.003)	NA	NA	NA
			Complete	0.243 (0.059)	0.321 (0.098)	0.965 (0.015)	0.153 (0.035)
(0.8, 0.6)	30	0.3	STORE	0.586 (0.055)	0.992 (0.109)	0.879 (0.016)	0.369 (0.035)
			MAGEE	1.515 (0.004)	NA	NA	NA
			Complete	0.555 (0.071)	0.898 (0.120)	0.852 (0.025)	0.269 (0.041)
			No-fusion	0.155 (0.007)	0.139 (0.008)	1.000 (0.000)	0.121 (0.001)
			POSTER	0.106 (0.006)	0.115 (0.009)	1.000 (0.000)	0.020 (0.003)
		0.7	STORE	0.593 (0.062)	0.948 (0.111)	1.000 (0.000)	0.074 (0.020)
			MAGEE	1.528 (0.004)	NA	NA	NA
			Complete	0.524 (0.064)	0.857 (0.118)	0.875 (0.019)	0.370 (0.047)
			No-fusion	0.156 (0.007)	0.151 (0.010)	0.885 (0.021)	0.328 (0.060)
			POSTER	0.143 (0.008)	0.139 (0.010)	1.000 (0.000)	0.000 (0.000)
	40	0.3	STORE	0.287 (0.055)	0.402 (0.104)	0.957 (0.013)	0.212 (0.028)
			MAGEE	1.310 (0.003)	NA	NA	NA
			Complete	0.222 (0.054)	0.327 (0.100)	0.961 (0.016)	0.094 (0.029)
			No-fusion	0.144 (0.007)	0.137 (0.008)	1.000 (0.000)	0.120 (0.000)
			POSTER	0.100 (0.006)	0.114 (0.009)	1.000 (0.000)	0.020 (0.003)
		0.7	STORE	0.228 (0.052)	0.281 (0.090)	1.000 (0.000)	0.054 (0.003)
			MAGEE	1.325 (0.003)	NA	NA	NA
			Complete	0.243 (0.059)	0.321 (0.098)	0.965 (0.015)	0.153 (0.035)

Table 2: Simulation example with random missing, for varying observation probability  $p$ , signal strength  $w_k$ , and fusion setting  $f_0$ . Reported are the average estimation errors of  $\mathcal{B}$  and of  $\beta_{k,j}$ , and the true and false positive rates of selection based on 30 data replications (the standard errors in the parentheses). Two methods are compared: our method without the fusion constraint (No-fusion), and our proposed method (POSTER).

$p$	$w_k$	$f_0$	method	Error of $\mathcal{B}$	Error of $\beta_{k,j}$	TPR	FPR
0.5	30	0.3	No-fusion	0.090 (0.001)	0.058 (0.001)	1.000 (0.000)	0.121 (0.001)
			POSTER	0.054 (0.001)	0.037 (0.001)	1.000 (0.000)	0.022 (0.003)
		0.7	No-fusion	0.088 (0.001)	0.056 (0.001)	1.000 (0.000)	0.093 (0.021)
			POSTER	0.078 (0.001)	0.051 (0.001)	1.000 (0.000)	0.074 (0.018)
	40	0.3	No-fusion	0.067 (0.001)	0.044 (0.001)	1.000 (0.000)	0.120 (0.000)
			POSTER	0.043 (0.001)	0.029 (0.001)	1.000 (0.000)	0.022 (0.003)
		0.7	No-fusion	0.066 (0.001)	0.043 (0.001)	1.000 (0.000)	0.072 (0.000)
			POSTER	0.059 (0.001)	0.038 (0.001)	1.000 (0.000)	0.055 (0.003)
0.3	30	0.3	No-fusion	0.195 (0.035)	0.340 (0.093)	0.980 (0.008)	0.261 (0.045)
			POSTER	0.079 (0.003)	0.222 (0.081)	0.979 (0.010)	0.140 (0.039)
		0.7	No-fusion	0.247 (0.049)	0.506 (0.113)	0.952 (0.014)	0.348 (0.055)
			POSTER	0.109 (0.004)	0.374 (0.104)	0.969 (0.013)	0.281 (0.054)
	40	0.3	No-fusion	0.112 (0.020)	0.104 (0.044)	0.995 (0.005)	0.130 (0.010)
			POSTER	0.059 (0.001)	0.087 (0.045)	0.996 (0.004)	0.034 (0.009)
		0.7	No-fusion	0.086 (0.002)	0.055 (0.001)	1.000 (0.000)	0.094 (0.021)
			POSTER	0.076 (0.001)	0.050 (0.001)	1.000 (0.000)	0.074 (0.020)

## 5.2 Random missing

In the second example, we simulate data similarly as in Section 5.1, but the entries of the response tensor are randomly missing. We set the observation probability  $p \in \{0.3, 0.5\}$ . For this setting, MAGEE cannot handle a tensor response with randomly missing entries, whereas STORE or our method applied to the complete data cannot handle either, since there is almost no complete  $\mathcal{Y}_i$ , with the probability of observing a complete  $\mathcal{Y}_i$  being  $p^{d_1 d_2 d_3 q}$ . Therefore, we can only compare our proposed method with the variation that imposes no fusion constraint. Table 2 reports the results based on 30 data replications. It is seen that incorporating the fusion structure clearly improves the estimation accuracy.

## 5.3 Model misspecification

In the third example, we simulate data from the model in Li et al. (2013). Data generated this way does not comply with our proposed model (1), and we examine the performance of our method under model misspecification. Following Li et al. (2013), we simulate a third-order tensor response  $\mathcal{Y}_i \in \mathbb{R}^{d_1 \times d_2 \times T}$ , where the first two modes correspond to imaging space and the third mode corresponds to the time dimension, with  $d_1 = d_2 = 88$ ,  $T = 3$ , and the sample

size  $n = 80$ . At voxel  $(j, k)$  the response of subject  $i$  at time point  $l$  is simulated according to

$$\mathcal{Y}_{i,j,k,l} = \mathbf{x}_{i,l}^\top \boldsymbol{\beta}_{j,k} + \epsilon_{i,j,k,l}, \quad i \in [n], l \in [3].$$

The predictor vector  $\mathbf{x}_{i,l} = (1, x_{i,l,2}, x_{i,l,3})^\top$ , and we consider two settings of generating  $\mathbf{x}_{i,l}$ . The first setting is that  $x_{i,l,2}$  is time-dependent and is generated from a uniform distribution on  $[l-1, l]$  for  $l = 1, 2, 3$ , and  $x_{i,l,3}$  is time independent and is generated from a Bernoulli distribution with probability 0.5. The second setting is that both  $x_{i,l,2}$  and  $x_{i,l,3}$  are time independent and are generated from a Bernoulli distribution with probability 0.5. The error term  $\boldsymbol{\epsilon}_{i,j,k} = (\epsilon_{i,j,k,1}, \epsilon_{i,j,k,2}, \epsilon_{i,j,k,3})^\top$  is generated from a multivariate normal  $N(0, \Sigma)$ , where the diagonal entries of  $\Sigma$  are 1 and  $\text{Corr}(\epsilon_{i,j,k,l_1}, \epsilon_{i,j,k,l_2}) = 0.7^{|l_1-l_2|}$ ,  $l_1, l_2 = 1, 2, 3$ . The coefficient  $\boldsymbol{\beta}_{j,k} = (0, \beta_{j,k,2}, \beta_{j,k,3})^\top$ , and the coefficient image is divided into six different regions with two different shapes. Following [Li et al. \(2013\)](#), we set  $(\beta_{j,k,2}, \beta_{j,k,3})$  to  $(0, 0)$ ,  $(0.05, 0.9)$ ,  $(0.1, 0.8)$ ,  $(0.2, 0.6)$ ,  $(0.3, 0.4)$  and  $(0.4, 0.2)$  in those six regions. Among the 80 subjects, the first half have their  $88 \times 88$  images observed only at the first two time points.

Figure 1 presents the true and estimated image of  $\beta_{j,k,2}$ , along with the estimation error of the coefficient tensor  $\boldsymbol{\beta}$ . The standard error shown in parenthesis is calculated based on 20 replications. The results for  $\beta_{j,k,3}$  are similar and hence are omitted. It is seen that our method is able to capture all six important regions in both settings of covariates, even if the model is misspecified. When the covariates are time independent, our estimator is more accurate compared to the method of [Li et al. \(2013\)](#). When the covariates are time dependent, our method performs worse, because it is not designed for time dependent covariates.

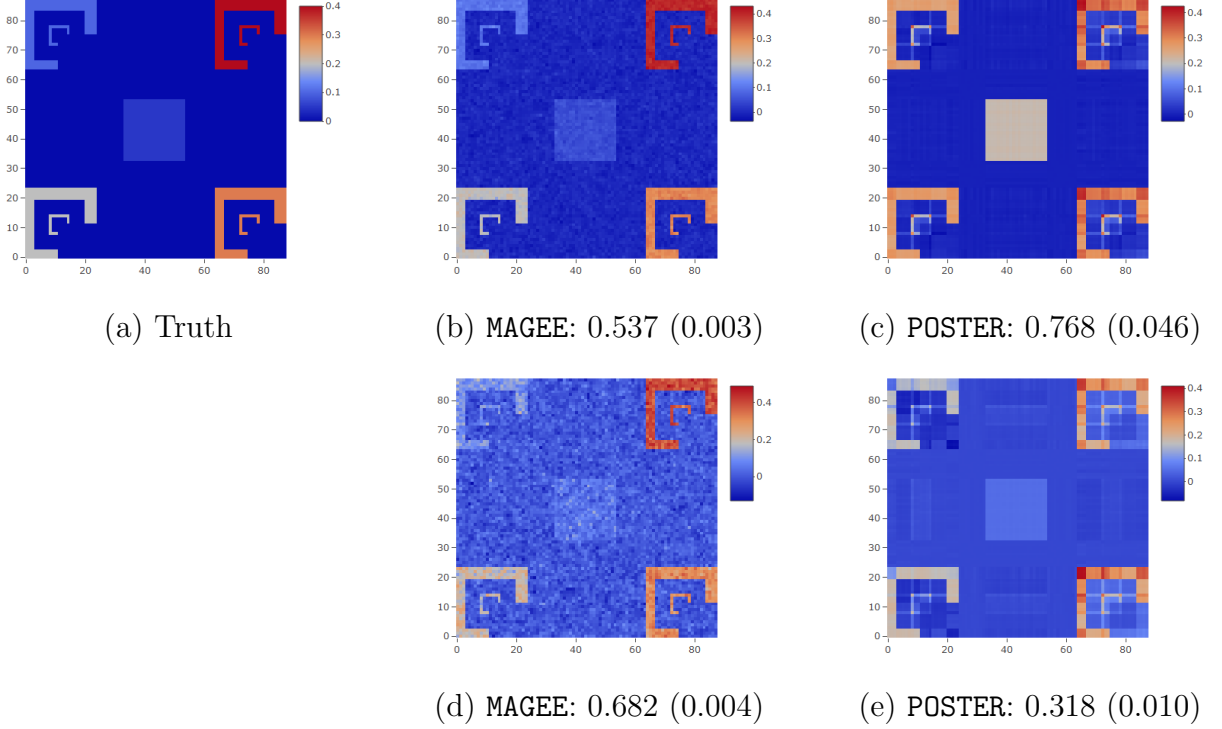
## 6 Applications

We illustrate the proposed method with two real data applications. The first is a neuroimaging study, where about 50% of subjects have at least one imaging scan missing. The second is a digital advertising study, where about 95% of tensor entries are missing.

### 6.1 Neuroimaging application

The first example is a neuroimaging study of dementia. Dementia is a broad category of brain disorders with symptoms associated with decline in ability to think and remember that is severe enough to affect a person's daily functioning ([Sosa-Ortiz et al., 2012](#)). It is of keen

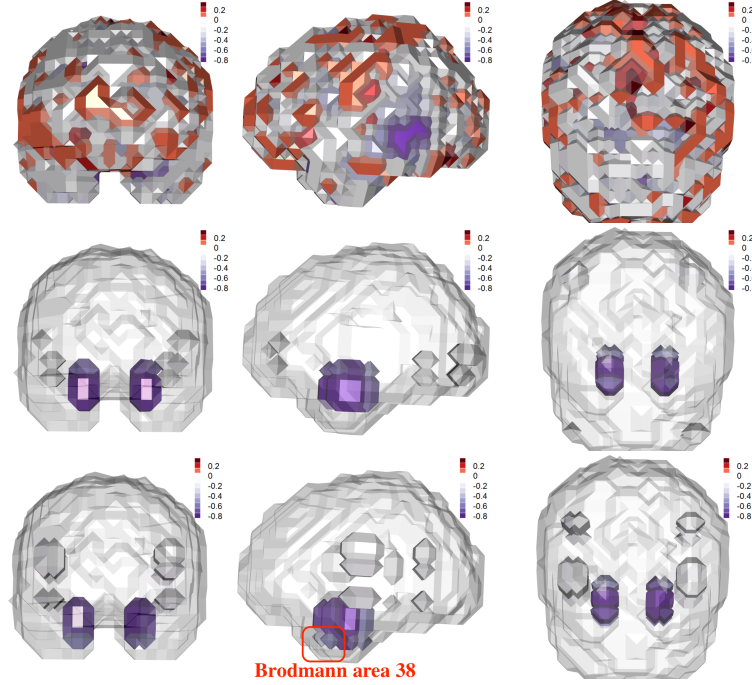
Figure 1: The image of  $\beta_{j,k,2}$ . The top left panel is the true image of  $\beta_{j,k,2}$  with six regions. The middle panels are the estimated images by **MAGEE**, and the right panels by our method **POSTER**. The top panels correspond to the time dependent covariates, and the bottom panels the time independent covariates. The estimation error (with the standard error in the parenthesis) based on 20 data replications is reported for each image.



scientific interest to understand how brain structures change and differ between dementia patients and healthy controls, which in turn would facilitate early disease diagnosis and development of effective treatment.

The data we analyze is obtained from the Alzheimer’s Disease Neuroimaging Initiative (ADNI, <http://adni.loni.usc.edu>). In this study, anatomical MRI brain images were collected from  $n = 365$  participants every six months over a two-year period. Each MRI image, after preprocessing and mapping to a common registration space, is summarized in the form of a  $32 \times 32 \times 32$  tensor. For each participant, there are at most five scans, but many subjects missed some scheduled scans, and 178 subjects out of 365 have at least one scan missing. For each subject, we stack the MRI brain images collected over time as a fourth-order tensor, which is to serve as the response  $\mathcal{Y}_i$ . Its dimension is  $32 \times 32 \times 32 \times 5$ , and there are block missing entries. Among these subjects, 127 have dementia and 238 are

Figure 2: Neuroimaging application example. Shown are the estimated coefficient tensor overlaid on a randomly selected brain image. Top to bottom: **MAGEE**, **STORE**, and our method **POSTER**. Left to right: frontal view, side view, and top view.



healthy controls. In addition, the baseline age and sex of the subjects were collected. As such, the predictor vector  $\mathbf{x}_i$  consists of the binary diagnosis status, age and sex. Our goal is to identify brain regions that differ between dementia patients and healthy controls, while controlling for other covariates.

We apply **MAGEE**, **STORE** and our **POSTER** method to this dataset. Figure 2 shows the heatmap of the estimated coefficient tensor obtained by the three methods, from top to bottom, respectively. It is seen that the estimate from **MAGEE** is noisy, which identifies a large number of regions with relatively small signals. Both **STORE** and **POSTER** identify several important brain regions, and the parameters in those identified regions are negative, indicating that those regions become less active for patients with dementia. The regions identified by the two methods largely agree with each other, with one exception, i.e., Brodmann area 38, which **POSTER** identifies but **STORE** does not. The regions identified by both include hippocampus and the surrounding medial temporal lobe. These findings are consistent with existing neuroscience literature. Hippocampus is found crucial in memory formation, and medial temporal lobe is important for memory storage (Smith and Kosslyn, 2007). Hippocampus is

commonly recognized as one of the first regions in the brain to suffer damages for patients with dementia (Hampel et al., 2008). There is also clear evidence showing that medial temporal lobe is damaged for dementia patients (Visser et al., 2002). In addition to those two important regions, our method also identifies a small part of the anterior temporal cortex, i.e., Brodmann area 38, which is highlighted in Figure 2. This area is involved in language processing, emotion and memory, and is also among the first areas affect by Alzheimer’s disease, which is the most common type of dementia (Delacourte et al., 1998).

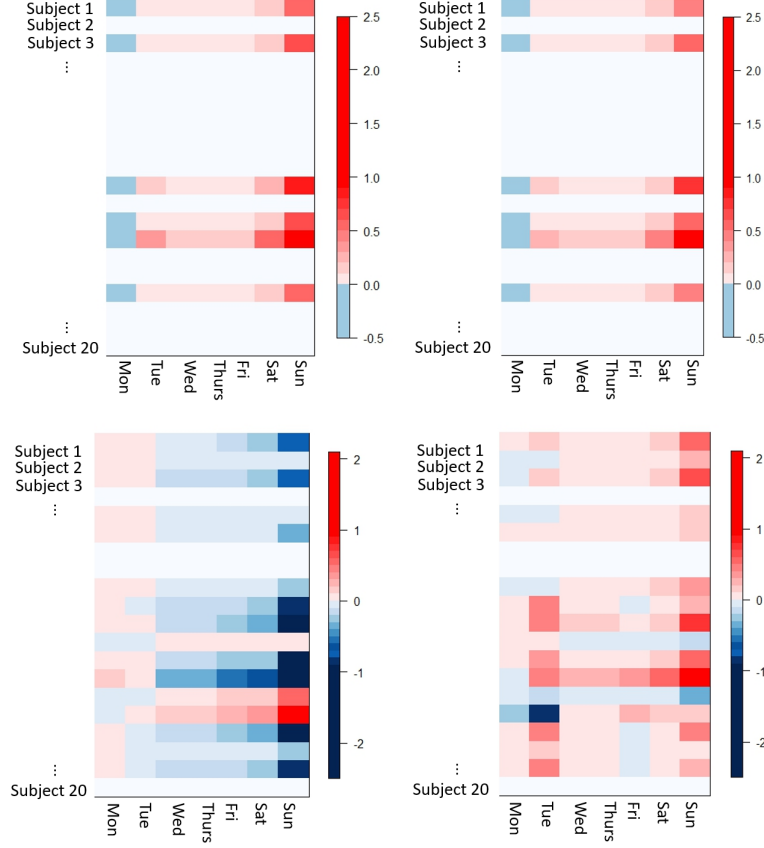
## 6.2 Digital advertising application

The second example is a digital advertising study of click-through rate (CTR) for some online advertising campaign. CTR is the number of times a user clicks on a specific advertisement divided by the number of times the advertisement is displayed. It is a crucial measure to evaluate the effectiveness of an advertisement campaign, and plays an important role in digital advertising pricing (Richardson et al., 2007).

The data we analyze is obtained from a major internet company over four weeks in May to June, 2016. The CTR of  $n = 80$  advertisement campaigns were recorded for 20 users by 2 different publishers. Since it is of more interest to understand the user behavior over different days of a week, the data were averaged by days of a week across the four-week period. For each campaign, we stack the CTR data of different users and publishers over seven days of the week as a third-order tensor, which is to serve as the response  $\mathcal{Y}_i$ . Its dimension is  $20 \times 2 \times 7$ , and there are 95% entries missing. Such a missing percentage, however, is not uncommon in online advertising, since a user usually does not see every campaign by every publisher everyday. For each campaign, we also observe two covariates. One covariate is the topic of the advertisement campaign, which takes three categorical values, “online dating”, “investment”, or “others”. The other covariate is the total number of impressions of the advertisement campaign. The predictor vector  $\mathbf{x}_i$  consists of these two covariates. Our goal is to study how the topic and total impression of an advertisement campaign affect its effectiveness measured by CTR.

Due to the large proportion of missing values and nearly random missing patterns, neither `MAGEE` nor `STORE` is applicable to this dataset. We apply our method. For the categorical covariate, topic, we create two dummy variables, one indicating whether the topic is “online

Figure 3: Digital advertising application example. Shown are the estimated coefficient tensor. In each panel, the rows represent users and columns represent days of a week. The top panels are for the topic “online dating”, and the bottom panels for “investment”. The left panels are slices from the topic mode, and the right panels are slices from the impression mode.



dating” or not, and the other indicating whether the topic is “investment” or not. Figure 3 shows the heatmap of the estimated coefficient tensor for one publisher, whereas the result for the other publisher is similar and is thus omitted. The rows of the heatmap represent the users and the columns represent the days of a week. We first consider the topic of “online dating”. The top left panel shows that, for this topic, the CTR is higher than other topics during the weekend. The top right panel shows that, if the total impression on “online dating” increases, then the CTR increases more on weekends than weekdays. Such patterns are consistent across different users. It is also interesting to see that the topic of “online dating” has a negative impact on the CTR on Mondays. We next consider the topic of “investment”. The bottom left panel shows that, for this topic, the CTR is lower than other topics for most users during the weekend; however, the CTR on this topic is higher on

Mondays and Tuesdays. The bottom right panel shows that, if the total impression increases, the CTR increases more on weekends than weekdays. These findings are useful for managerial decisions. Based on the findings about “online dating”, one should increase the allocation of “online dating” related advertisements on weekends, and decrease the allocation on Mondays. On the other hand, the allocation recommendation for “investment” related advertisements are different. For most users, one should allocate more such advertisements during the early days of a week, and fewer during weekends. For a small group of users who seem to behave differently from the majority, some personalized recommendation regarding “investment” advertisements can also be beneficial.

## References

- ANANDKUMAR, A., DENG, Y., GE, R. and MOBAHI, H. (2017). Homotopy analysis for tensor pca. *Conference on Learning Theory* 79–104.
- ANANDKUMAR, A., GE, R., HSU, D. and KAKADE, S. M. (2014). A tensor approach to learning mixed membership community models. *Journal of Machine Learning Research* **15** 2239–2312.
- BALAKRISHNAN, S., WAINWRIGHT, M. J. and YU, B. (2017). Statistical guarantees for the em algorithm: From population to sample-based analysis. *The Annals of Statistics* **45** 77–120.
- BRUCE, N. I., MURTHI, B. and RAO, R. C. (2017). A dynamic model for digital advertising: The effects of creative format, message content, and targeting on engagement. *Journal of marketing research* **54** 202–218.
- BULLMORE, E. and SPORNS, O. (2009). Complex brain networks: graph theoretical analysis of structural and functional systems. *Nature Reviews Neuroscience* **10** 186–198.
- CHEN, H., RASKUTTI, G. and YUAN, M. (2019). Non-convex projected gradient descent for generalized low-rank tensor regression. *Journal of Machine Learning Research* **20** 1–37.
- DELACOURTE, A., DAVID, J. ET AL. (1998). The biochemical pathway of neurofibrillary degeneration in aging and alzheimer’s disease. *American Academy of Neurology* **52** 1158–1165.

- FENG, X., LI, T., SONG, X. and ZHU, H. (2019). Bayesian scalar on image regression with non-ignorable non-response. *Journal of the American Statistical Association* .
- HAMPEL, H., BURGER, K. ET AL. (2008). Core candidate neurochemical and imaging biomarkers of alzheimer’s disease. *Alzheimer’s and Dementia*. **4** 38–48.
- JAIN, P. and OH, S. (2014). Provable tensor factorization with missing data. *Advances in Neural Information Processing Systems* **2** 1431–1439.
- KOLDA, T. G. and BADER, B. W. (2009). Tensor decompositions and applications. *SIAM review* **51** 455–500.
- LI, L. and ZHANG, X. (2017). Parsimonious tensor response regression. *Journal of the American Statistical Association* **112** 1131–1146.
- LI, Y., GILMORE, J. H., SHEN, D., STYNER, M., LIN, W. and ZHU, H. (2013). Multiscale adaptive generalized estimating equations for longitudinal neuroimaging data. *NeuroImage* **72** 91 – 105.
- MADRID-PADILLA, O. and SCOTT, J. (2017). Tensor decomposition with generalized lasso penalties. *Journal of Computational and Graphical Statistics* **26** 537–546.
- RABUSSEAU, G. and KADRI, H. (2016). Low-rank regression with tensor responses. In *Advances in Neural Information Processing Systems*.
- RASKUTTI, G. and YUAN, M. (2019). Convex regularization for high-dimensional tensor regression. *Annals of Statistics* **47** 1554–1584.
- RICHARDSON, M., DOMINOWSKA, E. and RAGNO, R. (2007). Predicting clicks: estimating the click-through rate for new ads. In *Proceedings of the 16th international conference on World Wide Web*. ACM.
- RINALDO, A. (2009). Properties and refinements of the fused lasso. *The Annals of Statistics* **37** 2922–2952.
- SHEN, X., PAN, W. and ZHU, Y. (2012). Likelihood-based selection and sharp parameter estimation. *Journal of American Statistical Association* **107** 223–232.
- SMITH, E. E. and KOSSLYN, S. M. (2007). Cognitive psychology: Mind and brian. *New Jersey: Prentice Hall*. **21** 279–306.

- SOSA-ORTIZ, A. L., ACOSTA-CASTILLO, I. and PRINCE, M. J. (2012). Epidemiology of dementias and alzheimer’s disease. *Archives of medical research* **43** 600–608.
- SUN, W., LU, J., LIU, H. and CHENG, G. (2017). Provable sparse tensor decomposition. *Journal of the Royal Statistical Society, Series B* **79** 899–916.
- SUN, W., WANG, Z., LIU, H. and CHENG, G. (2015). Non-convex statistical optimization for sparse tensor graphical model. In *Advances in Neural Information Processing Systems*.
- SUN, W. W. and LI, L. (2017). Store: Sparse tensor response regression and neuroimaging analysis. *Journal of Machine Learning Research* **18** 1–37.
- SUN, W. W. and LI, L. (2019). Dynamic tensor clustering. *Journal of American Statistical Association* **114** 1894 – 1907.
- TAN, K. M., WANG, Z., LIU, H. and ZHANG, T. (2018). Sparse generalized eigenvalue problem: optimal statistical rates via truncated rayleigh flow. *Journal of the Royal Statistical Society: Series B* **80** 1057–1086.
- THUNG, K.-H., WEE, C.-Y., YAP, P.-T. and SHEN, D. (2016). Identification of progressive mild cognitive impairment patients using incomplete longitudinal mri scans. *Brain Structure and Function* **221** 3979–3995.
- TIBSHIRANI, R., SAUNDERS, M., ROSSET, S., ZHU, J. and KNIGHT, K. (2005). Sparsity and smoothness via the fused lasso. *Journal of the Royal Statistical Society Series B* **67** 91–108.
- VISSER, P., VERHEY, F., HOFMAN, P. ET AL. (2002). Medial temporal lobe atrophy predicts alzheimer’s disease in patients with minor cognitive impairment. *Journal of Neurology, Neurosurgery and Psychiatry*. **72** 491–497.
- VOUNOU, M., NICHOLS, T. E., MONTANA, G., INITIATIVE, A. D. N. ET AL. (2010). Discovering genetic associations with high-dimensional neuroimaging phenotypes: A sparse reduced-rank regression approach. *Neuroimage* **53** 1147–1159.
- WANG, Y., SHARPNACK, J., SMOLA, A. and TIBSHIRANI, R. (2016). Trend filtering on graphs. *Journal of Machine Learning Research* **17** 1–41.
- WANG, Y., TUNG, H.-Y., SMOLA, A. and ANANDKUMAR, A. (2015a). Fast and guaranteed tensor decomposition via sketching. *Advances in Neural Information Processing Systems* .

- WANG, Z., GU, Q., NING, Y. and LIU, H. (2015b). High dimensional em algorithm: Statistical optimization and asymptotic normality. In *Advances in Neural Information Processing Systems*.
- XIA, D. and YUAN, M. (2017). On polynomial time methods for exact low rank tensor completion. *Foundations of Computational Mathematics* 1–49.
- XUE, F. and QU, A. (2019). Integrating multi-source block-wise missing data in model selection. *arXiv preprint, arXiv:1901.03797* .
- YIN, H., CUI, B., CHEN, L., HU, Z. and ZHOU, X. (2015). Dynamic user modeling in social media systems. *ACM Transactions on Information Systems* **33** 1–44.
- YUAN, M. and ZHANG, C. (2016). On tensor completion via nuclear norm minimization. *Foundations of Computational Mathematics* **16** 1031–1068.
- YUAN, M. and ZHANG, C. (2017). Incoherent tensor norms and their applications in higher order tensor completion. *IEEE Transactions on Information Theory* **63** 6753–6766.
- YUAN, X.-T. and ZHANG, T. (2013). Truncated power method for sparse eigenvalue problems. *Journal of Machine Learning Research* **14** 899–925.
- ZHANG, A. (2019). Cross: Efficient low-rank tensor completion. *Annals of Statistics* **47** 936–964.
- ZHANG, Z., ALLEN, G. I., ZHU, H. and DUNSON, D. (2019). Tensor network factorizations: Relationships between brain structural connectomes and traits. *NeuroImage* **197** 330–343.
- ZHOU, H., LI, L. and ZHU, H. (2013). Tensor regression with applications in neuroimaging data analysis. *Journal of the American Statistical Association* **108** 540–552.
- ZHU, H., CHEN, Y., IBRAHIM, J. G., LI, Y., HALL, C. and LIN, W. (2009). Intrinsic regression models for positive-definite matrices with applications to diffusion tensor imaging. *Journal of the American Statistical Association* **104** 1203–1212.
- ZHU, Y., SHEN, X. and PAN, W. (2014). Structural pursuit over multiple undirected graphs. *Journal of the American Statistical Association* **109** 1683–1696.